
Regiospecific Nucleation and Growth of Silane Coupling Agent Droplets onto Colloidal Particles

Marlous Kamp, Giuseppe Soligno, Fabian Hagemans, Bo Peng, Arnout Imhof,

René van Roij, Alfons van Blaaderen

– Supporting Information –

Dr. M. Kamp, F. Hagemans, Dr. B. Peng, Dr. A. Imhof, Prof. Dr. A. van Blaaderen

Soft Condensed Matter, Debye Institute for Nanomaterials Science, Utrecht University, Princetonplein 1, 3584 CC Utrecht, The Netherlands.

E-mail: M.Kamp@uu.nl, A.vanBlaaderen@uu.nl

Dr. G. Soligno, Prof. Dr. R. van Roij

Institute for Theoretical Physics, Utrecht University, Princetonplein 5, 3584 CC Utrecht, The Netherlands.

† These authors contributed equally.

1 Supplementary Figures

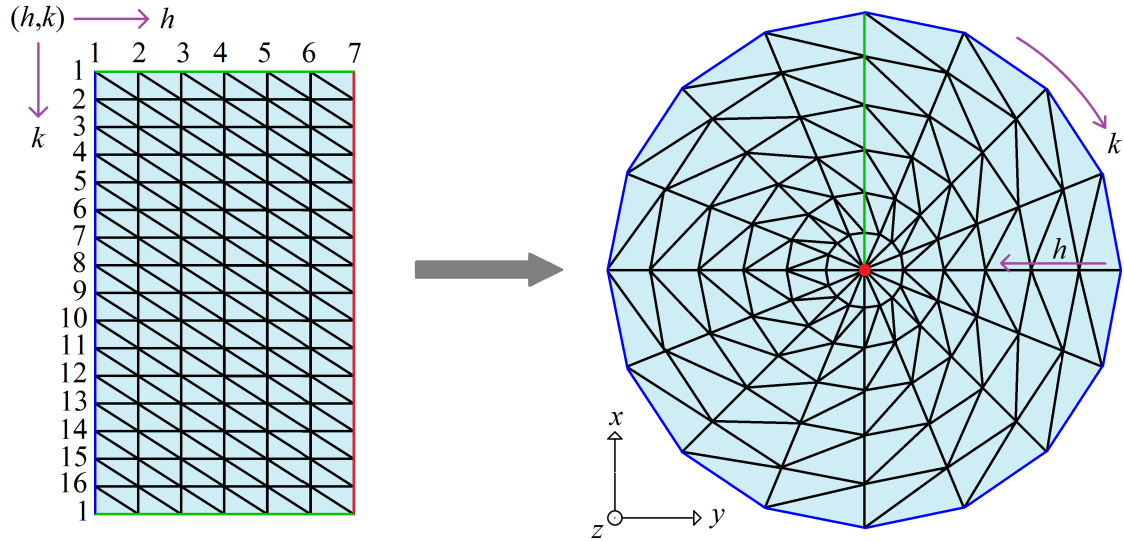


Figure S1: Sketch of a 16×7 point grid to represent the fluid-fluid interface of a droplet. The number of points used here is just illustrative, since the fluid-fluid interface grids used for the calculations in this paper had roughly 30 points in the polar direction of the droplet and 100 points in the azimuthal direction. Using Monte Carlo simulations, we move these grid points in the 3D space to find their position with minimum free energy, keeping constant the volume of the droplet (given as an input parameter). The droplet is attached at a colloidal particle with a given surface, so the points of the grid with $h=1$ are constrained to move only on the particle surface. The points with highest h ($h=7$ in this sketch) coincide in a single point and are moved all together and only along the vertical (z) direction, during the Monte Carlo simulation. All the other points of the grid are freely moved in the 3D space, but keeping constant their azimuthal angle with respect to the vertical axis passing through the center of the grid.

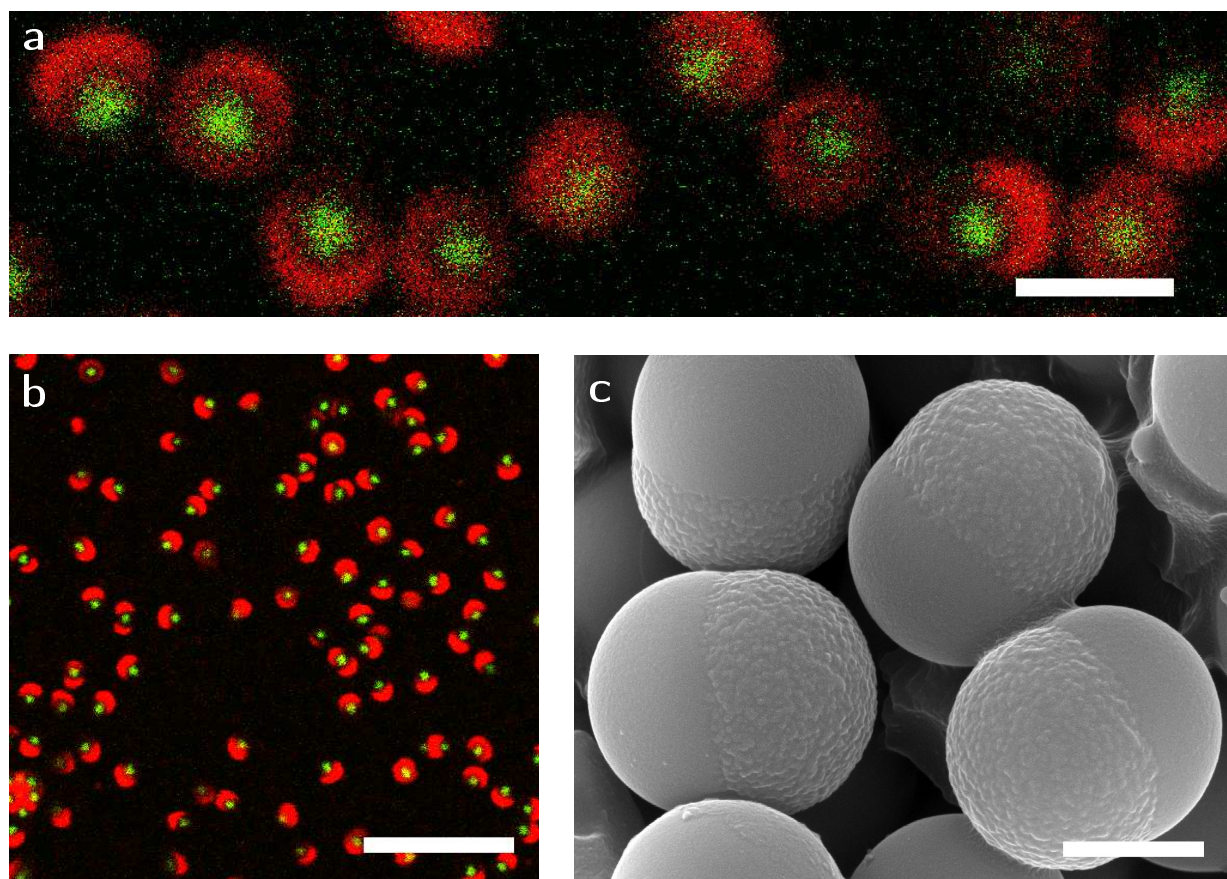


Figure S2: (a,b) Confocal micrographs and (c) Scanning Electron Microscopy (SEM) image of dumbbell-shaped silica/MPTMS* hetero-dimers, reproduced from the work of Sacanna/Pine and coworkers^[s1]. Panel (a) is a close-up of silica/MPTMS* particles to display the cap-like shape of the dyed MPTMS* bulge (rhodamine labeled, displayed in red). Note that the fluorescent core (fluoresceine labeled, displayed in green) of the silica particle is enveloped in a non-fluorescent shell, which is not visible. Scale bars denote 2 μm , 10 μm and 1 μm , respectively.

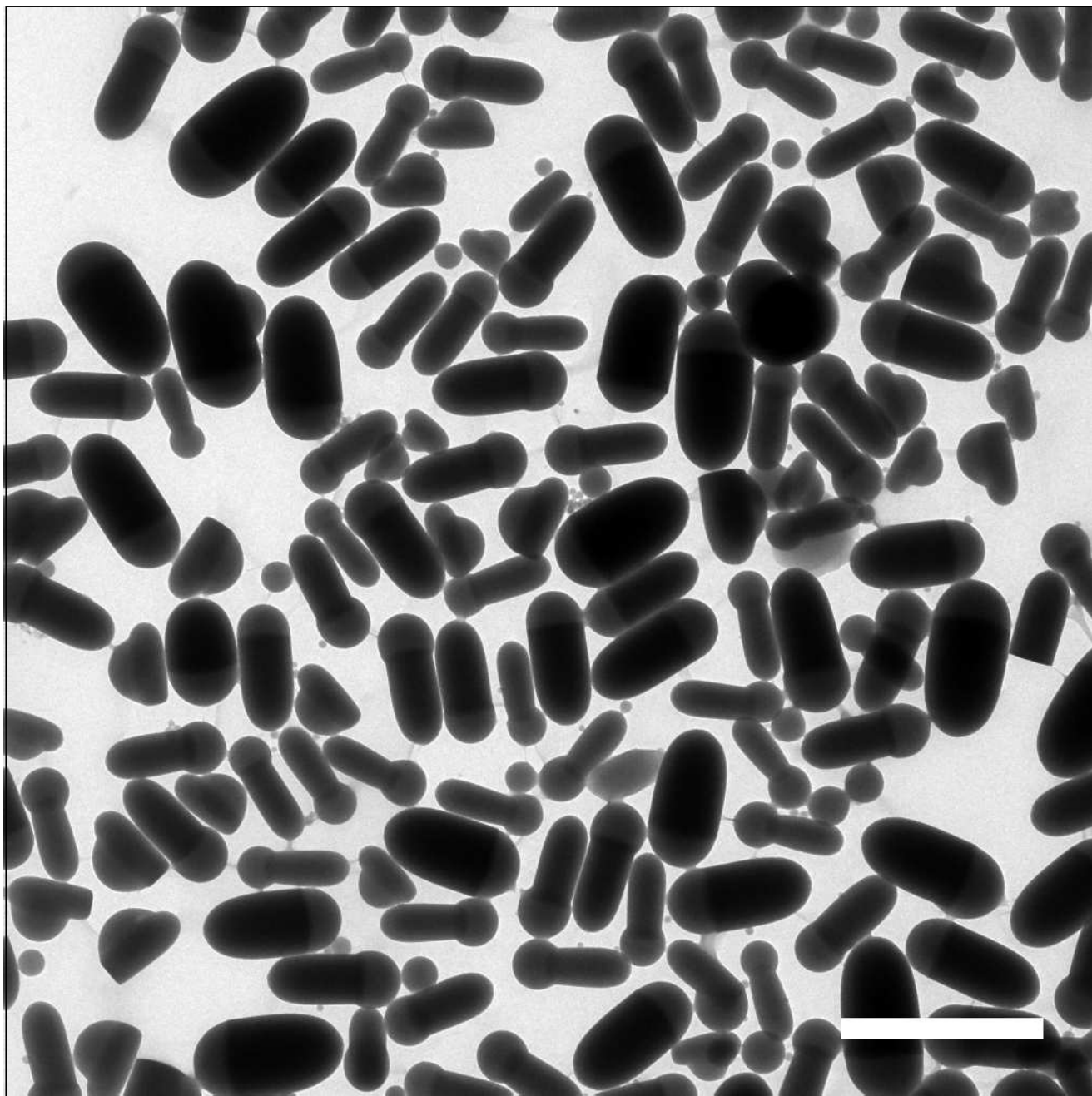


Figure S3: Transmission Electron Microscopy image of hetero-dimer particles prepared by nucleation and growth of MPTMS^* onto OTMS-grafted short bullet-shaped particles (aspect ratio $m = 2.1 \pm 0.1$, with standard deviation $\sigma_m = 0.4$).

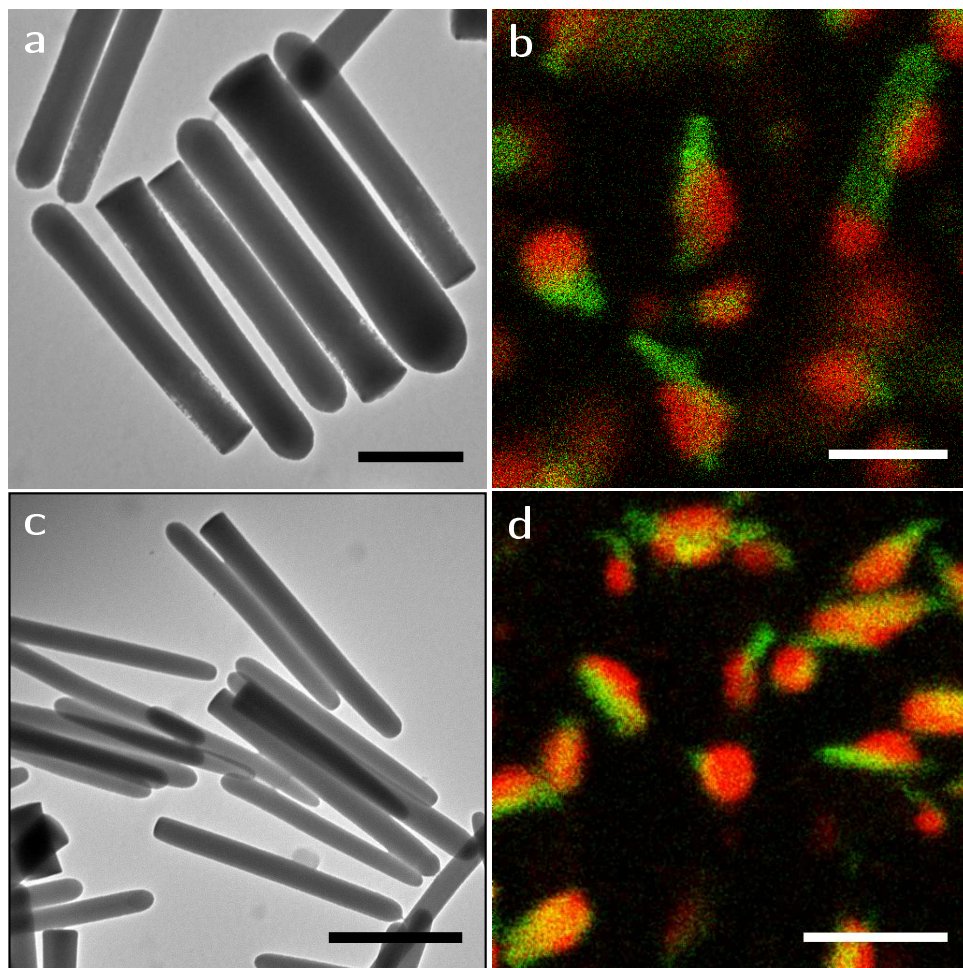


Figure S4: **Nucleation and growth for intermediate and high aspect ratio bullet-shaped template particles: edge-on attachment.** (a) TEM and (b) Confocal micrograph of bullet-shaped particles (aspect ratio $m = 6.2 \pm 0.2$, $\sigma_m = 1.0$) (a) before and (b) after dye labeling, OTMS-grafting and MPTMS* nucleation and condensation. Note the end-on attached MPTMS* droplet on the particle on the top right (which was the only such particle we found in our sample) and the side-on attachment of all other MPTMS* droplets. The scale bars denote: (a) $1 \mu\text{m}$, and (b) $2 \mu\text{m}$. (c) TEM and (d) Confocal micrograph of bullet-shaped particles (aspect ratio $m = 10.1 \pm 0.1$, $\sigma_m = 0.9$) (c) before and (d) after dye labeling, OTMS-grafting and MPTMS* nucleation and condensation. The scale bars denote: (c) $1 \mu\text{m}$, and (d) $4 \mu\text{m}$.

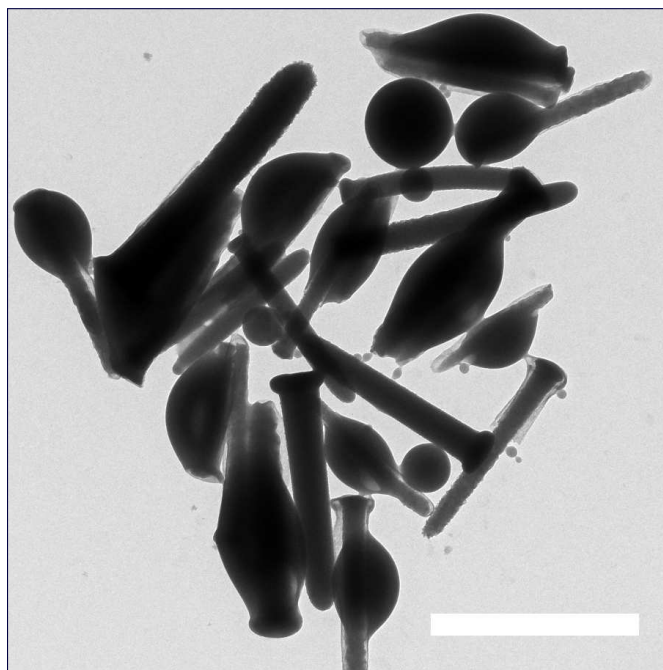


Figure S5: Hetero-dimers prepared by nucleation and growth of MPTMS* onto OTMS-grafted, long nail-shaped particles ($m = 8.6 \pm 0.4$, $\sigma_m = 2$). MPTMS* failed to nucleate onto the flat end for these high aspect ratio template particles. Scale bar: 2 μm .

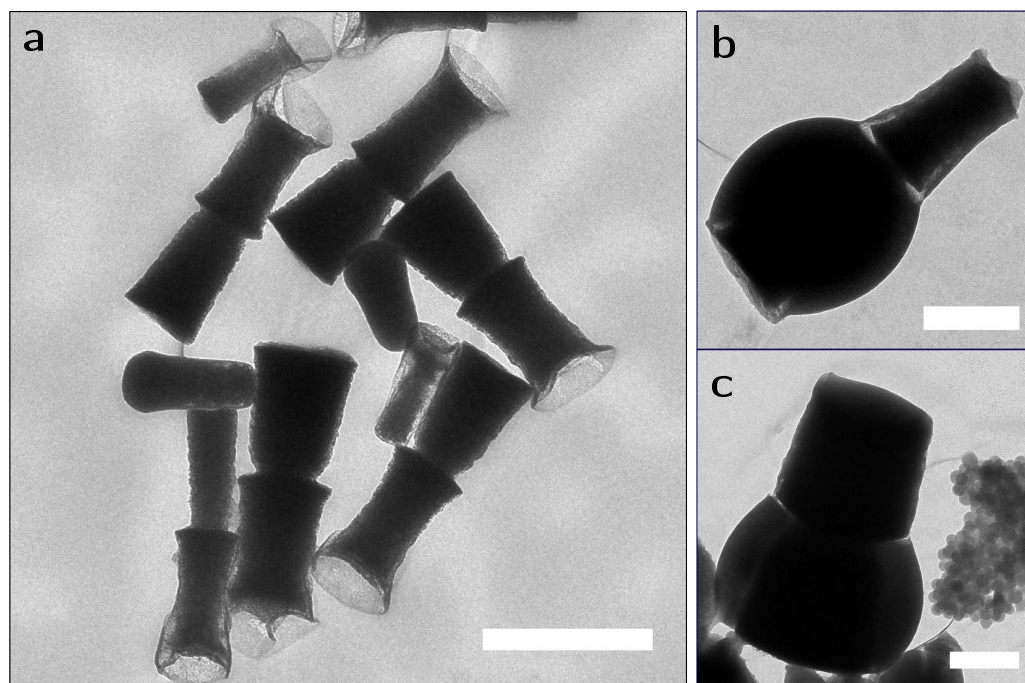


Figure S6: Transmission Electron Microscopy images of (a) Silica double cones. (b,c) Hetero-dimers corresponding to the double cones in (a). Scale bars represent (a) 1 μm , and (b,c) 500 nm.

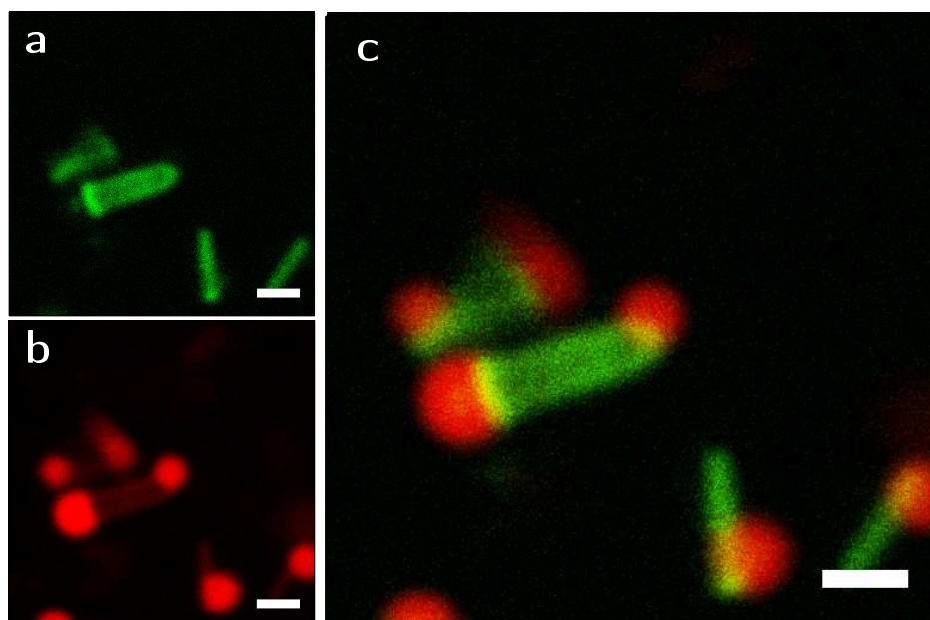


Figure S7: Confocal micrographs of the same sample as in Figure 1, showing lollipop-shaped hetero-dimers with an extra MPTMS* droplet attached. (a) is the channel recording at 510 - 540 nm (around the emission maximum of FITC dye), (b) is the channel recording at 565 - 700 nm (around the emission maximum of RAS dye), and (c) is an overlay of both imaging channels. The scale bars denote 1 μm .

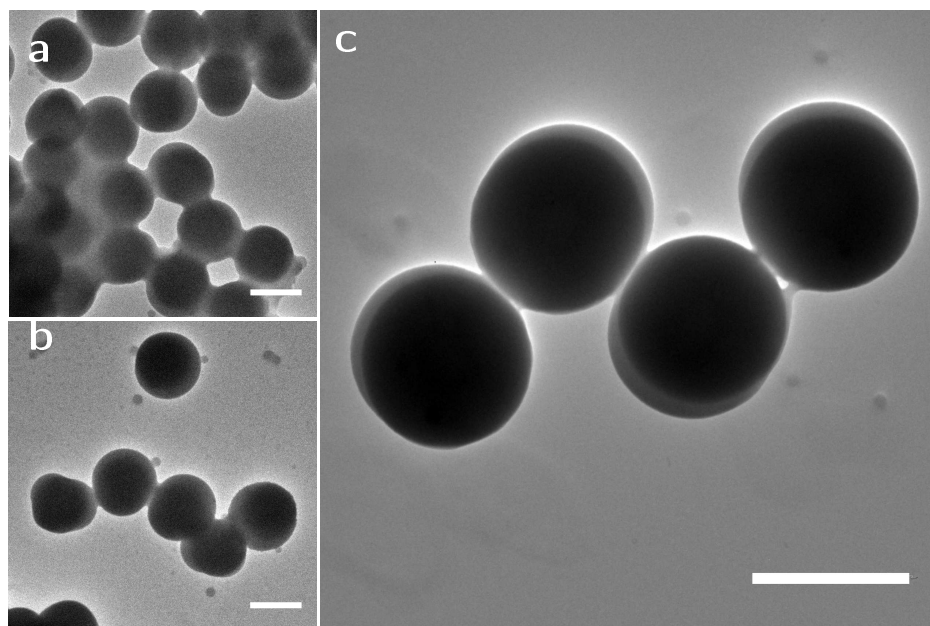


Figure S8: **Nucleation and growth of MPTMS* onto other surface graftings than OTMS.** TEM images of the product of a reaction in which MPTMS* was nucleated and grown onto silica particles (a,b) without a surface-grafting, (c) with an MPTMS grafting. Specifically, to 18 mg of (a,b) non-grafted or (c) MPTMS-grafted silica particles in 2.875 mL deionized water was added 1.14 mL of a solution of 0.35 wt.% F108 in water. After sonication of this dispersion, 4 μL ammonia and 70 μL MPTMS were added. The particles were cross-linked as follows: after 1 h of stirring, 6 mg AIBN was added, and after a further 10 min. stirring, the dispersion was heated to 70 $^{\circ}\text{C}$ overnight and washed three times with water. The scale bars represent 1 μm .

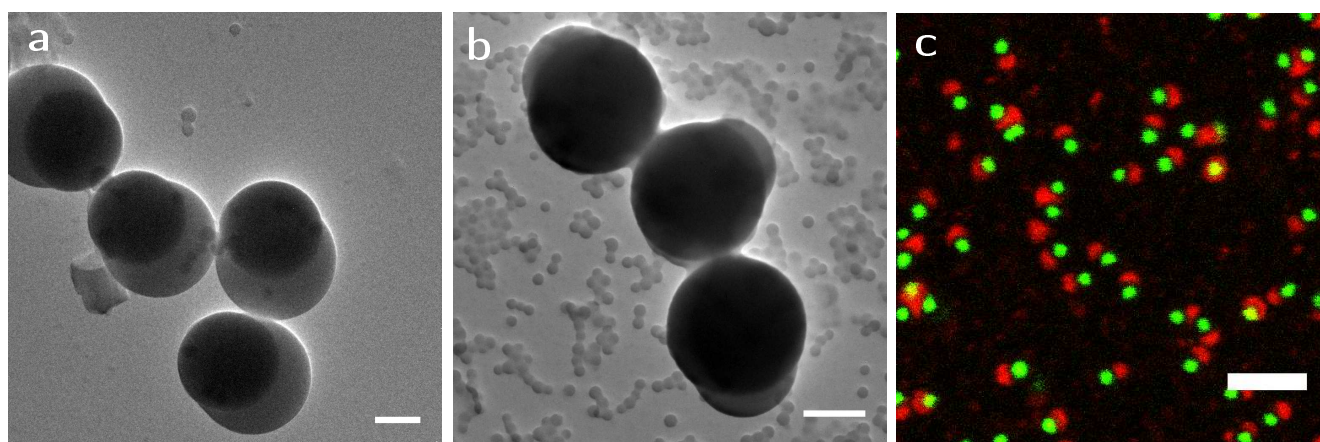


Figure S9: **Nucleation and growth of MPTMS* onto OTMS-grafted silica, using other surfactants than Pluronic F108.** (a,b) TEM images of dumbbell-shaped silica/MPTMS* hetero-dimers, prepared with (a) Pluronic F108 surfactant and (b) Triton X-100 surfactant instead of Pluronic F108 surfactant. Scale bars denote 0.5 μm . (c) Confocal micrograph of dumbbell-shaped silica/MPTMS* hetero-dimers, prepared with Igepal CO-520 surfactant instead of Pluronic F108 surfactant. These composite dumbbells did not remain intact during the cross-linking step. Scale bar denotes 2 μm .

2 Supplementary Theoretical Results

Particle surface definition

In the calculations presented in this paper, we considered three shapes for the colloidal particles, a nail of aspect ratio $m = 5.8$ (see Figure 3a), a bullet of aspect ratio $m = 6.0$ (see Figure 3b), and a bullet of aspect ratio $m = 2.1$ (see Figure 3c). The surface of each of these shape is defined using a triangular tessellated grid of 400×400 points. The generic position $\mathbf{p} = (p_x, p_y, p_z)$ of each point of the particle grid is defined using the following parametric equations

$$\begin{aligned} p_x/\xi &= a s[\cos(u\pi - \pi/2) \cos(2v\pi)] |\cos(2v\pi)| |\cos(u\pi - \pi/2)|^\epsilon \\ p_y/\xi &= a s[\cos(u\pi - \pi/2) \sin(2v\pi)] |\sin(2v\pi)| |\cos(u\pi - \pi/2)|^\epsilon \\ p_z/\xi &= b s[\sin(u\pi - \pi/2)] |\sin(u\pi - \pi/2)| + m - 1 \end{aligned} \quad (4)$$

where ξ is the unit length, corresponding to the radius of the cylindrical part of the particle, and $u, v \in [0, 1]$,

$$b = \begin{cases} 1, & \text{if } u\pi - \pi/2 > 0, \\ 2m - 1, & \text{otherwise;} \end{cases} \quad (5)$$

$$\epsilon = \begin{cases} 1.0, & \text{if } u\pi - \pi/2 > 0, \\ 0.05, & \text{otherwise;} \end{cases} \quad (6)$$

and

$$s(x) = \begin{cases} 1, & \text{if } x \geq 0, \\ -1, & \text{if } x < 0. \end{cases} \quad (7)$$

For the bullet-shaped particles $a = 1$, while for the nail-shaped particle

$$a = \begin{cases} 1.3, & \text{if } u\pi < 0.4, \\ 1, & \text{otherwise;} \end{cases} \quad (8)$$

The value of m corresponds to the desired aspect ratio for the particle (2.1 and 6.0 for the two bullet-shaped particles, respectively, and 5.8 for the nail-shaped particle).

Nail-shaped particle with aspect ratio $m = 5.8$

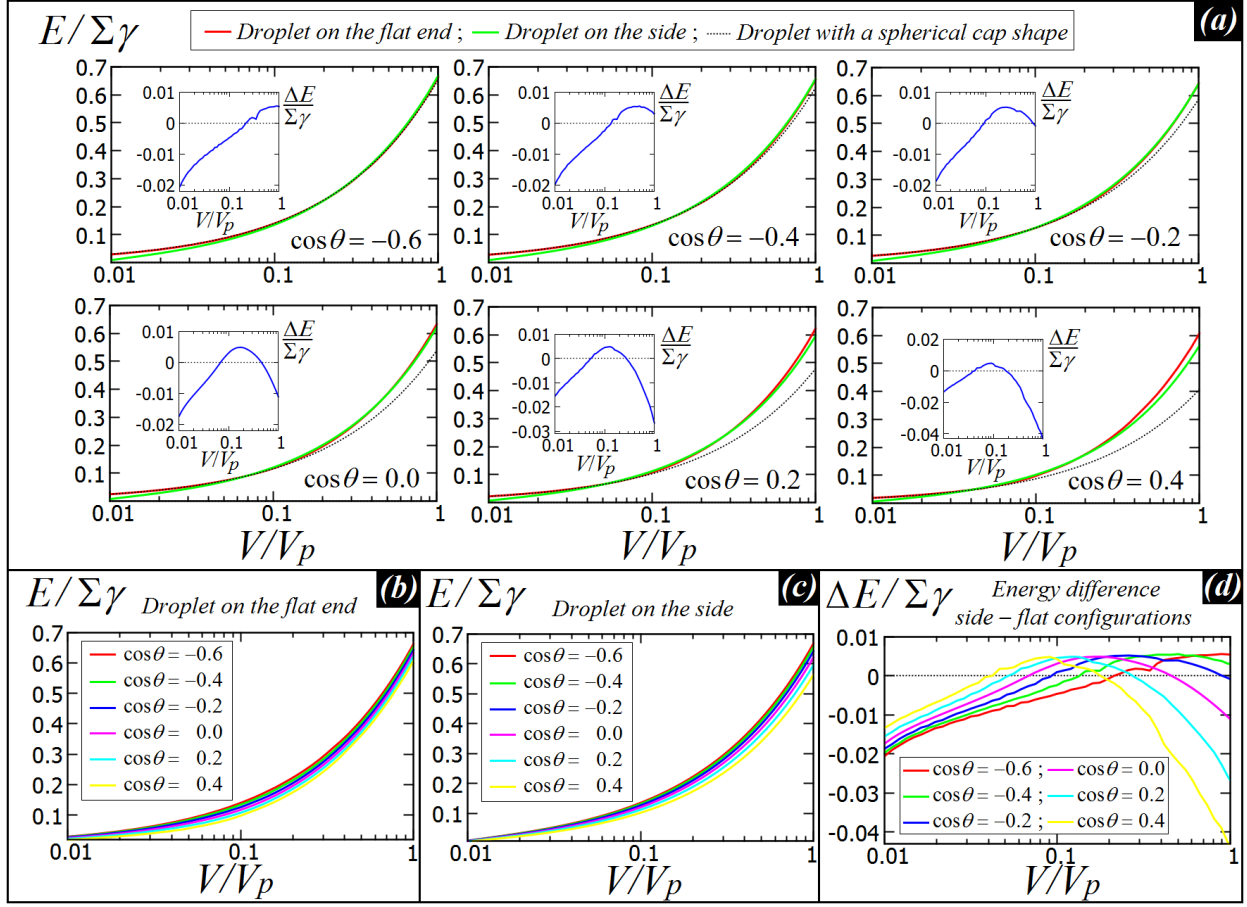


Figure S10: (a) Energy E (Equation 3) of a droplet in contact with a nail-shaped particle with aspect ratio $m = 5.8$ (see Figure 3d), with respect to the droplet volume V and for various Young's contact angles θ . V_p is the particle volume, and Σ is the particle total surface area. In Table S1, we report the value of $\Sigma\gamma$ in units of $k_B T$, for typical experimental parameters. The red line represents the case of a droplet attached to the flat end of the particle. The green line represents the case of a droplet attached to the long side of the particle. The dotted line is the energy $E(V)$ of a droplet with such contact angle and a spherical cap shape (from Equation 9). As expected, for small volumes the dotted line matches the red line corresponding to the energy of the droplet attached at the flat end. For such volumes indeed the droplet is not large enough to reach the edge of the particle, and so it assumes a spherical cap shape, as it lies on a flat substrate. In the insets we report the difference ΔE between the energy E of the droplet attached at the particle long side and the energy E of the droplet attached at the particle flat end (i.e. the difference between the green curve and the red curve). Therefore where $\Delta E > 0$ the configuration of the droplet attached at the particle flat end is the most convenient, while the droplet prefers to stay at the particle side where $\Delta E < 0$. In (b) and (c) the energy E (Equation 3) of the droplet attached respectively at the flat end and at the side of the particle is shown for the various Young's contact angles θ considered. In (d) the difference between the energy in (c) and the energy in (b) is shown.

Bullet-shaped particle with aspect ratio $m = 6.0$

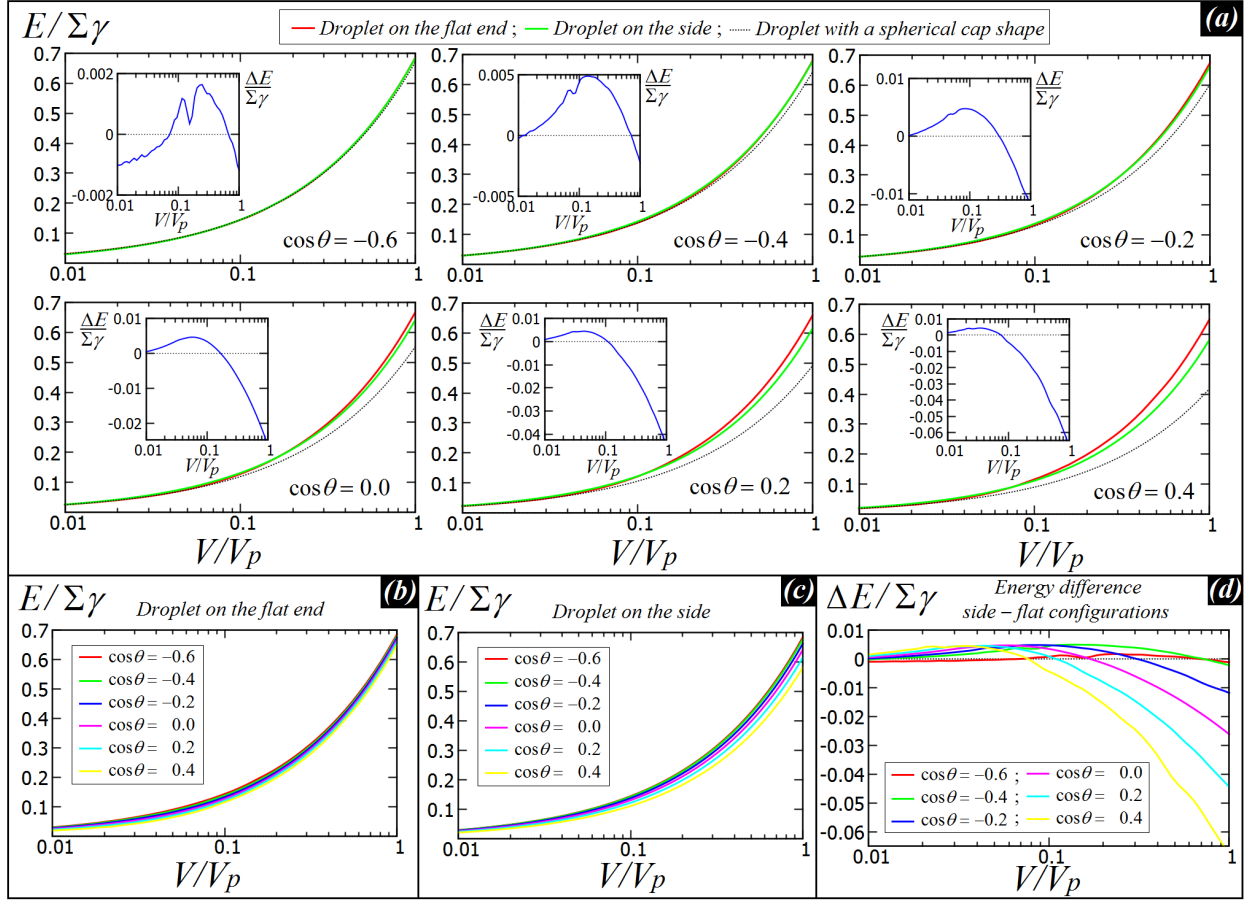


Figure S11: (a) Energy E (Equation 3) of a droplet in contact with a bullet-shaped particle with aspect ratio $m = 6.0$ (see Figure 3e), with respect to the droplet volume V and for various Young's contact angles θ . V_p is the particle volume, and Σ is the particle total surface area. In Table S1, we report the value of $\Sigma\gamma$ in units of $k_B T$, for typical experimental parameters. The red line represents the case of a droplet attached to the flat end of the particle. The green line represents the case of a droplet attached to the long side of the particle. The dotted line is the energy $E(V)$ of a droplet with such contact angle and a spherical cap shape (from Equation 9). As expected, for small volumes the dotted line matches the red line corresponding to the energy of the droplet attached at the flat end. For such volumes indeed the droplet is not large enough to reach the edge of the particle, and so it assumes a spherical cap shape, as it lies on a flat substrate. In the insets we report the difference ΔE between the energy E of the droplet attached at the particle long side and the energy E of the droplet attached at the particle flat end (i.e. the difference between the green curve and the red curve). Therefore where $\Delta E > 0$ the configuration of the droplet attached at the particle flat end is the most convenient, while the droplet prefers to stay at the particle side where $\Delta E < 0$. In (b) and (c) the energy E (Equation 3) of the droplet attached respectively at the flat end and at the side of the particle is shown for the various Young's contact angles θ considered. In (d) the difference between the energy in (c) and the energy in (b) is shown.

Bullet-shaped particle with aspect ratio $m = 2.1$

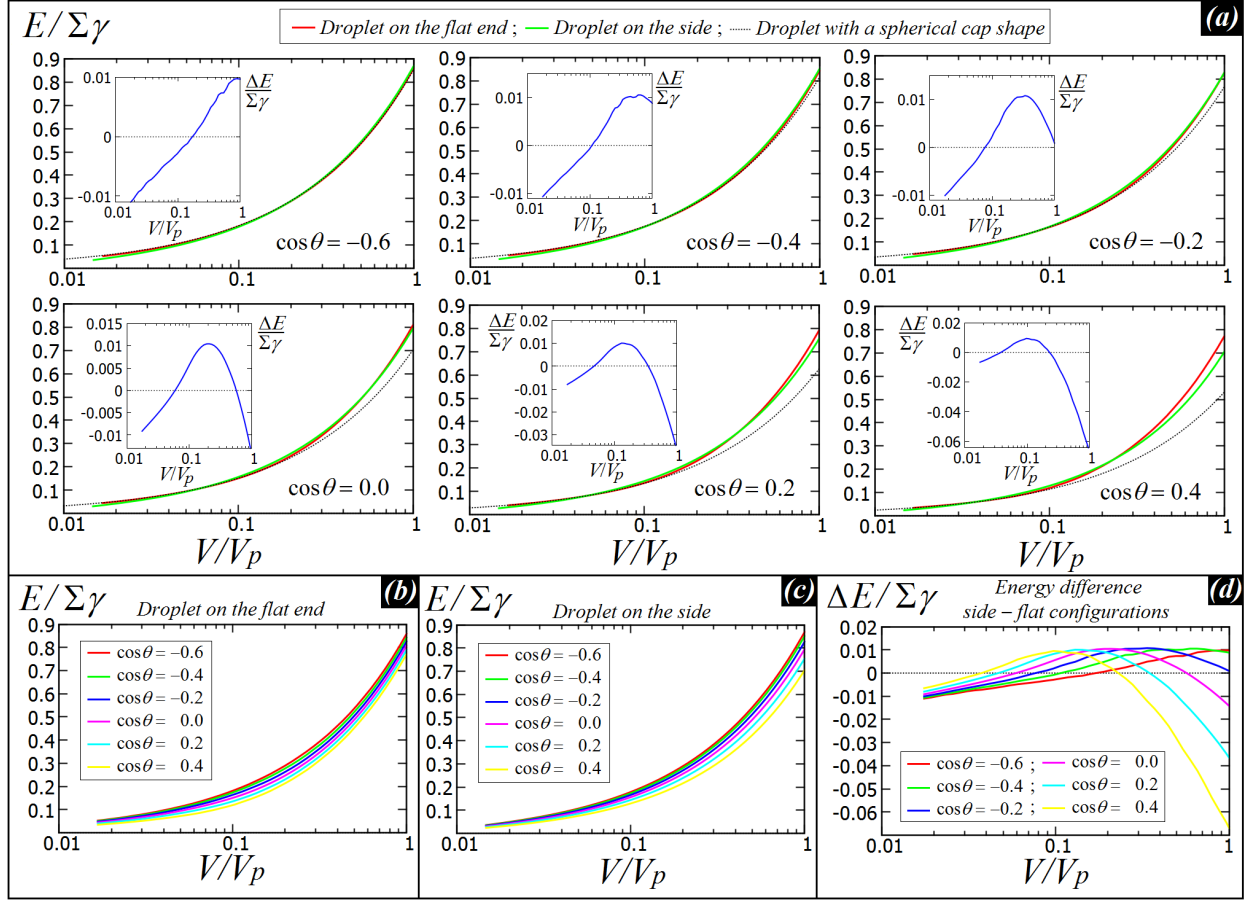


Figure S12: (a) Energy E (Equation 3) of a droplet in contact with a bullet-shaped particle with aspect ratio $m = 2.1$ (see Figure 3f), with respect to the droplet volume V and for various Young's contact angles θ . V_p is the particle volume, and Σ is the particle total surface area. In Table S1, we report the value of $\Sigma\gamma$ in units of $k_B T$, for typical experimental parameters. The red line represents the case of a droplet attached to the flat end of the particle. The green line represents the case of a droplet attached to the long side of the particle. The dotted line is the energy $E(V)$ of a droplet with such contact angle and a spherical cap shape (from Equation 9). As expected, for small volumes the dotted line matches the red line corresponding to the energy of the droplet attached at the flat end. For such volumes indeed the droplet is not large enough to reach the edge of the particle, and so it assumes a spherical cap shape, as it lies on a flat substrate. In the insets we report the difference ΔE between the energy E of the droplet attached at the particle long side and the energy E of the droplet attached at the particle flat end (i.e. the difference between the green curve and the red curve). Therefore where $\Delta E > 0$ the configuration of the droplet attached at the particle flat end is the most convenient, while the droplet prefers to stay at the particle side where $\Delta E < 0$. In (b) and (c) the energy E (Equation 3) of the droplet attached respectively at the flat end and at the side of the particle is shown for the various Young's contact angles θ considered. In (d) the difference between the energy in (c) and the energy in (b) is shown.

Nail-shaped particle with aspect ratio $m = 5.8$

In the next image (Figure S13), we show the 3D equilibrium shape of the droplet (as obtained numerically from our method) in its equilibrium configuration, i.e. at the particle side or at the particle flat end.

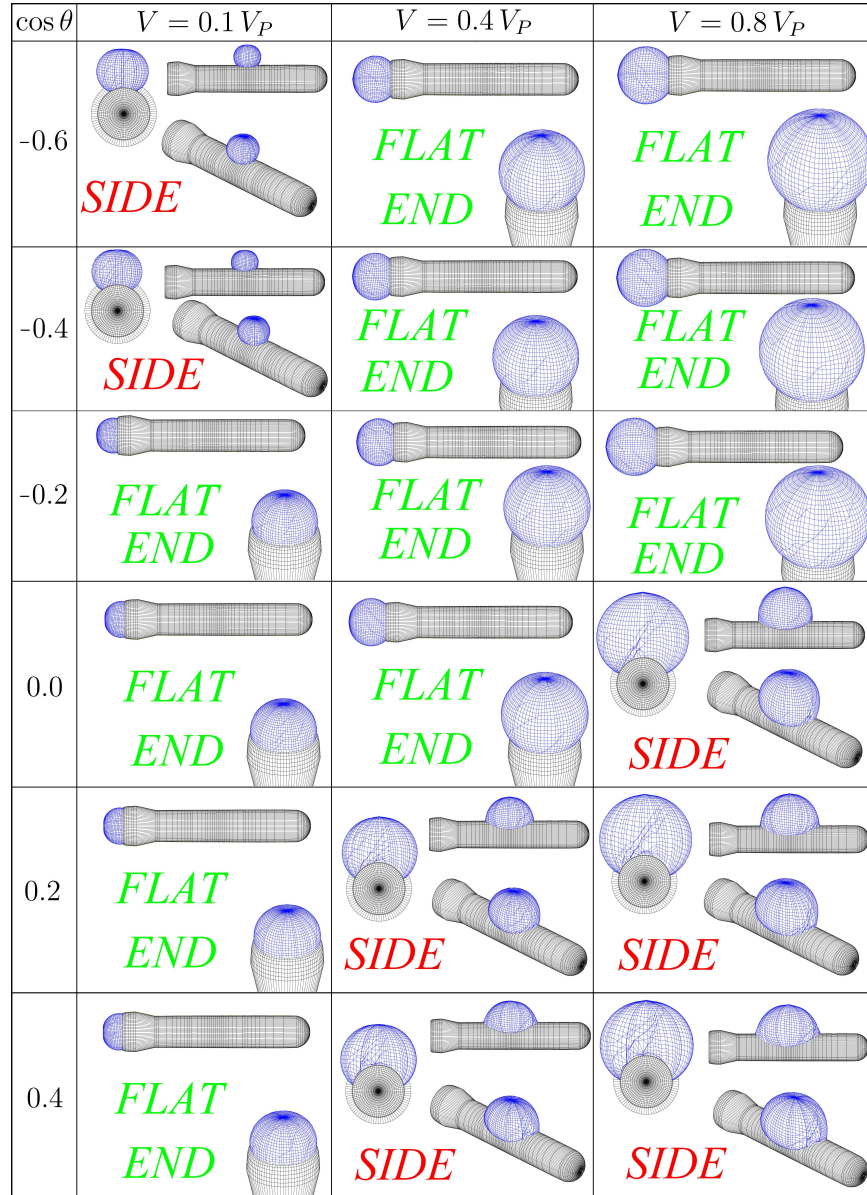


Figure S13: Three-dimensional view of the droplet equilibrium shape (as obtained numerically from our method) in its equilibrium configuration for the nail-shaped particle with aspect ratio 5.8, for $V = 0.1V_p$, $0.4V_p$, $0.8V_p$ and $\cos \theta = -0.6, -0.4, -0.2, 0.0, 0.2, 0.4$.

Bullet-shaped particle with aspect ratio $m = 6.0$

In the next image (Figure S14) we show the 3D equilibrium shape of the droplet (as obtained numerically from our method) in its equilibrium configuration, i.e. at the particle side or at the particle flat end.

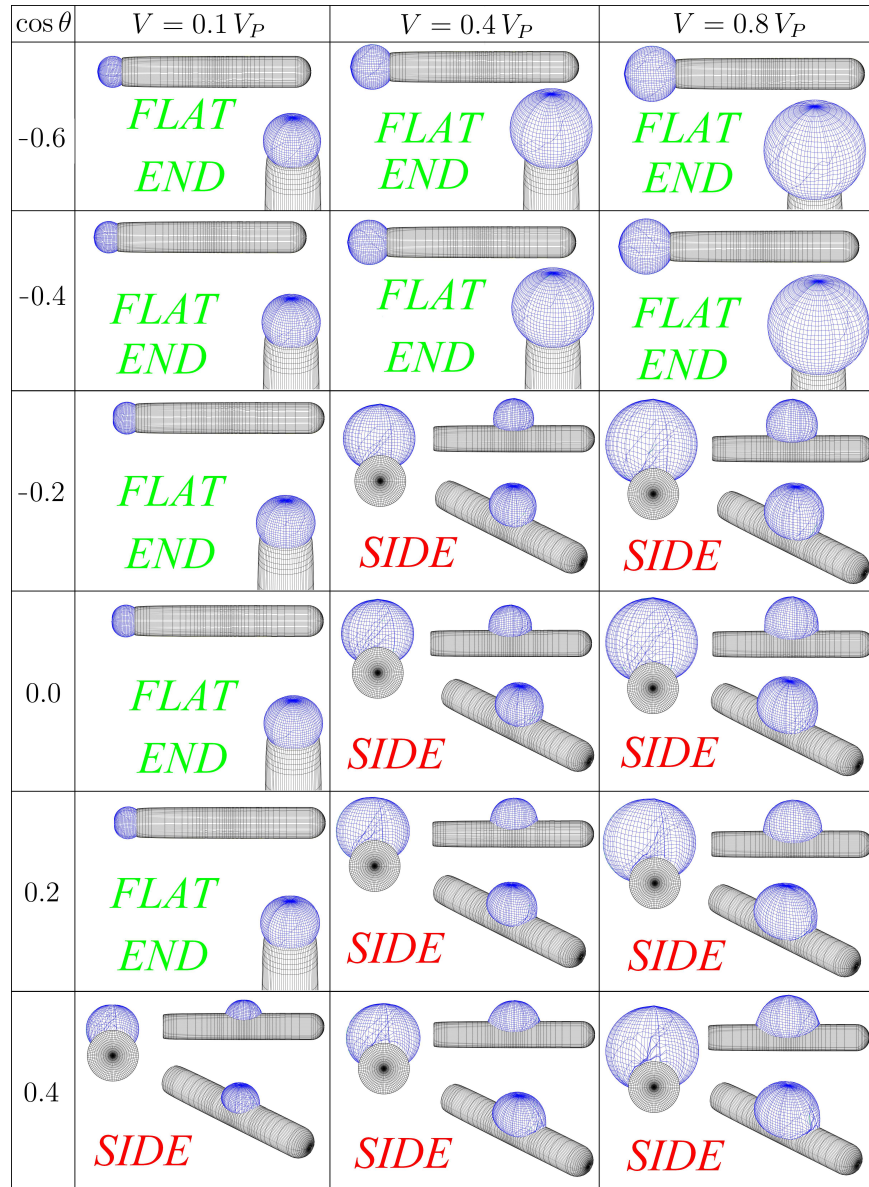


Figure S14: Three-dimensional view of the droplet equilibrium shape (as obtained numerically from our method) in its equilibrium configuration, i.e. attached at the particle side or at the particle flat end, for $V = 0.1V_p, 0.4V_p, 0.8V_p$ and $\cos \theta = 0.6, 0.4, 0.2, 0.0, 0.2, 0.4$, for the bullet-shaped particle with aspect ratio $m = 6.0$.

Bullet-shaped particle with aspect ratio $m = 2.1$

In the next image (Figure S15) we show the 3D equilibrium shape of the droplet (as obtained numerically from our method) in its equilibrium configuration, i.e. at the particle side or at the particle flat end.

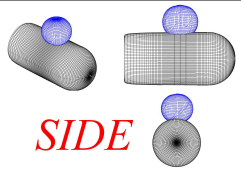
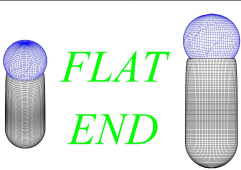
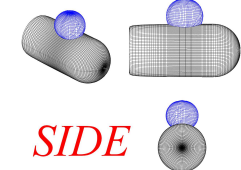
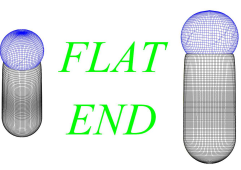
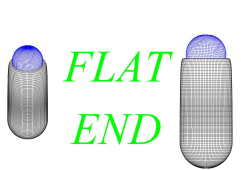
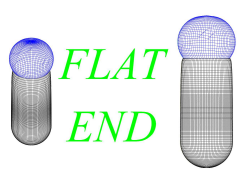
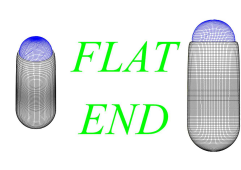
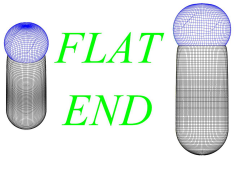
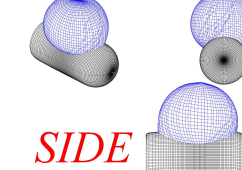
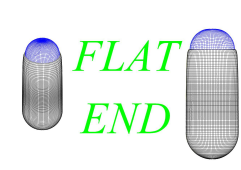
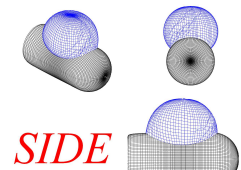
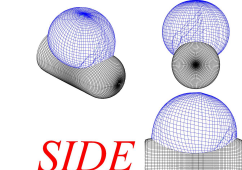
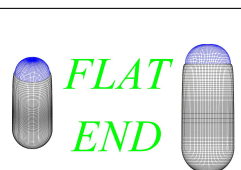
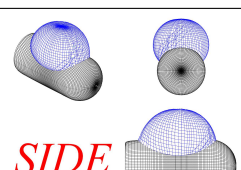
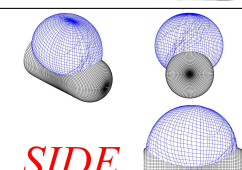
$\cos \theta$	$V = 0.1 V_P$	$V = 0.4 V_P$	$V = 0.8 V_P$
-0.6			
-0.4			
-0.2			
0.0			
0.2			
0.4			

Figure S15: Three-dimensional view of the droplet equilibrium shape (as obtained numerically from our method) in its equilibrium configuration, i.e. attached at the particle side or at the particle flat end, for $V = 0.1V_p, 0.4V_p, 0.8V_p$ and $\cos \theta = 0.6, 0.4, 0.2, 0.0, 0.2, 0.4$, for the bullet-shaped particle with aspect ratio 2.1.

2.1 Spherical cap-shaped droplets

When a droplet lies on a flat hard substrate, and the effects of gravity are negligible, it assumes the shape of a spherical cap (see Figure S16) with contact angle determined by Young's Law. The energy E (Equation (3)) of a droplet with a spherical cap shape of volume V and contact angle θ is

$$E(V, \theta) = \gamma [S(V, \theta) - \cos \theta W(V, \theta)] , \quad (9)$$

where $S(V, \theta) = 2\pi(1 - \cos \theta)R^2(V, \theta)$ is the fluid-fluid interface area of the spherical cap-shaped droplet, and $W(V, \theta) = \pi[R(V, \theta) \sin \theta]^2$ the solid-droplet interface area. Therefore

$$E(V, \theta) = \gamma \left[2(1 - \cos \theta) - \cos \theta (\sin \theta)^2 \right] \pi R^2(V, \theta) . \quad (10)$$

The volume of a spherical cap is

$$V = \left(\frac{2 + \cos \theta}{3} \right) (1 - \cos \theta)^2 \pi R^3 , \quad (11)$$

from which

$$R(V, \theta) = \sqrt[3]{\frac{3V}{\pi(2 + \cos \theta)(1 - \cos \theta)^2}} . \quad (12)$$

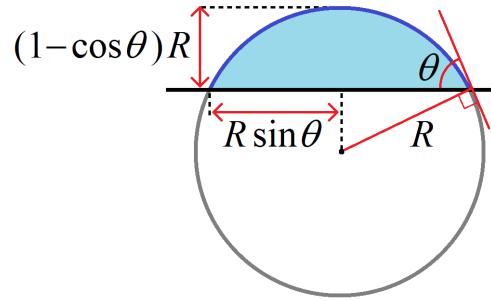


Figure S16: Section of a spherical cap with curvature radius R and Young's contact angle θ .

2.2 Tables

Values of $\Sigma\gamma$			
γ	$\Sigma\gamma/k_B T$ (for $\Sigma \approx 1.58 \mu\text{m}^2$)	$\Sigma\gamma/k_B T$ (for $\Sigma \approx 1.84 \mu\text{m}^2$)	$\Sigma\gamma/k_B T$ (for $\Sigma \approx 3.63 \mu\text{m}^2$)
0.005 N/m	$1.9 \cdot 10^6$	$2.2 \cdot 10^6$	$4.4 \cdot 10^6$
0.01 N/m	$3.8 \cdot 10^6$	$4.5 \cdot 10^6$	$8.8 \cdot 10^6$
0.02 N/m	$7.6 \cdot 10^6$	$9.0 \cdot 10^6$	$1.8 \cdot 10^7$

Table S1: Here we report the values of $\Sigma\gamma$ in units of $k_B T$ (at room temperature), for a given fluid-fluid surface tension γ and for a total particle surface area Σ of, respectively, $\Sigma \approx 1.58 \mu\text{m}^2$ (corresponding to the surface area of a bullet-shaped particle with aspect ratio 2.1 and cylinder diameter $0.47 \mu\text{m}$), $\Sigma \approx 1.84 \mu\text{m}^2$ (corresponding to the surface area of a bullet-shaped particle with aspect ratio 6.0 and cylinder diameter $0.31 \mu\text{m}$), and $\Sigma \approx 3.63 \mu\text{m}^2$ (corresponding to the surface area of a nail-shaped particle with aspect ratio 5.8, cylinder diameter $0.43 \mu\text{m}$ and nail-head diameter $0.56 \mu\text{m}$). This shows that the energy difference $\Delta E = \mathcal{O}(0.01 \Sigma\gamma)$ in Figure S7, S9, S11 is of the order of $10^4 - 10^6 k_B T$, for the considered values of γ . Typical values for the surface tension of an MPTMS-grafted silica surface against water are 37-39 N/m⁴⁴, however we expect that in our reaction mixture the surface tension is lowered by the presence of the surfactant F108. Moreover, no data are known for a hydrolyzing MPTMS* droplet.

γ	$\gamma_1 - \gamma_2$ (for $\cos \theta = \pm 0.2$)	$\gamma_1 - \gamma_2$ (for $\cos \theta = \pm 0.4$)	$\gamma_1 - \gamma_2$ (for $\cos \theta = \pm 0.6$)
0.005 N/m	$\pm 0.001 \text{ N/m}$	$\pm 0.002 \text{ N/m}$	$\pm 0.003 \text{ N/m}$
0.01 N/m	$\pm 0.002 \text{ N/m}$	$\pm 0.004 \text{ N/m}$	$\pm 0.006 \text{ N/m}$
0.02 N/m	$\pm 0.004 \text{ N/m}$	$\pm 0.008 \text{ N/m}$	$\pm 0.012 \text{ N/m}$

Table S2: Here we report, for a given fluid-fluid surface tension γ , the difference between the particle-external fluid surface tension γ_1 and the droplet-particle surface tension γ_2 , necessary to obtain the desired contact angle θ (measured inside the droplet), as obtained from Young's Law $\cos \theta = (\gamma_1 - \gamma_2) / \gamma$.

3 Supplementary Methods

Synthesis of dumbbell-shaped silica/MPTMS particles:* Dumbbell-shaped silica/MPTMS* particles (with an OTMS-grafted silica side and an MPTMS* lobe) were prepared according to a procedure given in Ref. s1. Silica particles (size: $970 \pm 5 \text{ nm}$, 2% p.d.) with a non-fluorescent shell grown by the method of Giesche *et al.*^[s2] around fluorescein isothiocyanate (FITC)-labeled silica seed particles of $\sim 300 \text{ nm}$ in diameter served as template particles. The particles were grafted with OTMS using the recipe described in the Experimental Section.

MPTMS was then hydrolyzed in water by a base-catalyzed reaction, in which a surfactant (Pluronic

F108) was added to influence the contact angle of the MPTMS* with the grafted surface. The liquid MPTMS* droplets nucleate and grow onto the OTMS-silica surface. In a typical synthesis, 18 mg of OTMS-grafted silica particles - dried from ethanol - were redispersed in a mixture of 2.875 mL water and 1.14 mL 0.35 wt.% Pluronic F108 in water by sonication in an ultrasonic bath (Branson 2510 or 8510) in a 20 mL glass vial. Under magnetic stirring, 4 μ L aqueous ammonia and subsequently 70 μ L MPTMS were added. MPTMS* droplets attached to the OTMS-silica were noticeable within 15 - 20 minutes. The shape of the MPTMS* lobe with this recipe was cap-like. The MPTMS* lobes were dyed as in the Experimental Section. After 1 h stirring with the dye solution, the methacrylate groups of the MPTMS* were cross-linked by adding 6 mg of AIBN, stirring for 10 minutes, and heating overnight at 70°C in an oil bath.

The shape of the hetero-dimer particles was successfully varied by using different surfactants in the nucleation and growth step. Adding a 0.35 wt.% aqueous solution of either Igepal CO-520 or Triton X-100 instead of Pluronic F108 solution resulted in a more pronounced/desorbed dumbbell shape than Pluronic F108. The particles prepared with Igepal CO-520 did not remain intact in an attempted cross-linking step.

4 Supplementary References

- [s1] Wang, Y.; Wang, Y.; Zheng, X.; Yi, G.-R.; Sacanna, S.; Pine, D.J.; Weck, M. Three-Dimensional Lock and Key Colloids. *J. Am. Chem. Soc.* **2014**, *136*, 6866 - 6869.
- [s2] Giesche, H. Synthesis of Monodispersed Silica Powders II. Controlled Growth Reaction and Continuous Production Process. *J. Eur. Ceram. Soc.* **1994**, *14*, 205 - 214.
- [s3] Liu, B. ; Besseling, T. H.; Hermes, M.; Demirörs, A.F.; Imhof, A.; van Blaaderen, A. Switching Plastic Crystals of Colloidal Rods with Electric Fields. *Nat. Commun.* **2014**, *5*, 3092(1) - 3092(4).
- [s4] Yan, J.; Han, M.; Zhang, J.; Xu, C.; Luijten, E.; Granick, S. Reconfiguring Active Particles by Electrostatic Imbalance. *Nat. Mater.* **2016**, *15*, 1095 - 1099.